Title
Lithium Batteries with Small-Molecule Quinone Cathode Enabled by Lithium Garnet Separators

Journal
ACS Applied Energy Materials, 6(2)

ISSN
2574-0962

Authors
Jonson, Robert A
Battaglia, Vincent S
Tucker, Michael C

Publication Date
2023-01-23

DOI
10.1021/acsaem.2c02932

Lithium Batteries with Small-Molecule Quinone Cathode Enabled by Lithium Garnet Separators

Robert A. Jonson[a], Vincent S. Battaglia[a], and Michael C. Tucker[a*]

[a]Lawrence Berkeley National Laboratory, 1 Cyclotron Road, Berkeley CA 94720, USA

*E-mail: mctucker@lbl.gov

Hybrid solid state battery, lithium metal battery, lithium garnet, LLZO, quinone, organic cathode

Abstract

The lithium garnet solid electrolyte (LLZO) provides an opportunity to consider cathode active materials which are not compatible with the conventional cell architecture based on porous separators and liquid electrolytes. For example, the class of organic materials known as quinones offer high specific capacities (up to 496 mAh/g), but are soluble in liquid electrolytes, leading to rapid capacity degradation. This work demonstrates solid electrolyte/liquid catholyte hybrid battery cells with metallic Li alloy as the anode and lawsone, a biologically-derived quinone, as the cathode. LLZO is used as a separator and effectively prevents dissolved cathode material from meeting the anode. Lawsone LLZO hybrid cells reached cathode utilization of up to 67% and had little self-discharge compared to liquid cells. Side reactions at voltages below 2.0 V limited their long-term cycling stability, however. Utilizing a lower cutoff voltage of 2.0 V or higher dramatically reduces capacity fade, but prevents complete lithiation of the second lawsone carbonyl group, curtailing capacity to only *ca.* 120 mAh/g. LLZO cells using 1,4-naphthoquinone, which is structurally identical to lawsone except for the absence of the irreversible hydroxyl lithiation site, were more stable at low voltages. These results suggest that achieving full theoretical capacity in a lawsone LLZO cell will require elimination of the low voltage side reactions to enable full utilization of both carbonyl groups, and mitigation of issues stemming from irreversible lithiation of the hydroxyl group. Nevertheless, use of a solid electrolyte is shown to be a promising approach to enable use of soluble organic cathode active materials.

Introduction

Quinones are among the more interesting organic materials being explored for use as cathode materials in Li batteries. Quinones offer several advantages compared to conventional inorganic cathode materials. They have high specific capacity (up to 496 mAh/g for 1,4-benzoquinone); contain no metal atoms and many can be biologically derived or sustainably synthesized; and, they can be used with many

battery chemistries including Li, Na, Mg and Zn.[1–4] Unfortunately, quinones generally have low ionic and electronic conductivity necessitating high cathode-side carbon and catholyte content, and low molecular weight quinones can dissolve into liquid electrolytes and cause cell failure. Common strategies to avoid dissolution include binding quinones to polymers,[5] or synthesizing larger, less soluble quinone molecules.[6] The resulting high molecular weight leads to lower volumetric and specific capacity compared to the underlying small molecule quinone materials. Senoh *et al.* developed an alternative two-compartment cell which used a lithium conducting glass-ceramic membrane to separate electrode chambers containing liquid-electrolyte.[7] Here, the lithium garnet ceramic solid electrolyte $Li_{6.25}AL_{.25}La_3Zr_2O_{12}$ (LLZO) is used as an impermeable membrane to block unwanted transport of dissolved small quinone molecules in a hybrid cell with solid electrolyte and liquid catholyte.

LLZO has attracted a lot of attention as an electrolyte material for next-generation solid-state lithium batteries because of its combination of high ionic conductivity (>1mS/cm at room temperature),[8,9] stability against Li metal anodes,[10,11] wide electrochemical window (>6 V),[12–14] applications in flexible composite electolytes,[15] and nonflammability. Practical battery systems using LLZO electrolytes, however, have been difficult to achieve because of a number of challenges, among them the creation of a stable, low impedance solid-state interface between the LLZO and cathode materials.[9,16] For example, common commercial cathodes such as $LiFePO_4$, $LiMn_2O_4$, $LiCoO_2$, and NMCs react and form high-impedance interfaces with LLZO at temperatures < 700°C preventing co-sintering of the materials as a way to form strong bonding.[17] Lower temperature in-situ synthesis of cathode materials from metal salts infiltrated into LLZO scaffolds has been found to create good bonding, however, it is difficult to achieve practical cathode loadings with this technique.[18] One widely-used method of achieving high loading is to adopt a hybrid cell configuration which uses some amount of polymer or liquid catholyte as a low impedance interface material.[19–23] This last approach is used here to demonstrate the combination of LLZO and quinone.

Of particular interest are hybrid cells with LLZO separator and liquid catholyte, using sulfur as a cathode. This cathode material suffers from a dissolution-based degradation mechanism known as the polysulfide shuttle,[24] which is similar in concept to that experienced with quinone cathodes. In these hybrid cells, LLZO blocks transport of dissolved polysulfides to the anode side.[25–28] Reported sulfur utilization in the first cycle was 74%[25] to 38%[26] and capacity retention was 88.4% over 9 cycles[25], 77.5% over 32 cycles[26], or 62.3% over 200 cycles.[27] Naguib *et al.* claim incomplete utilization was due to dissolution of sulfur to polysulfides, and formation of a reactive interfacial layer between the LLZO and liquid catholyte.[28]

The LLZO hybrid cells in this work predominantly use 2-hydroxy-1,4-naphthoquinone (lawsone, LS) which is a dye commonly extracted from the henna plant. LS has a reversible capacity of 307 mAh/g based on lithiation of its two carbonyl groups. It was selected both for its potentially sustainable plant-based source, and its electronic and ionic conductivities which are over an order of magnitude higher than similar quinone molecules, such as 1,4-naphthoquinone and 2-methyl-1,4-

naphthoquinone.[29] LS has been infiltrated at low loading into a carbon gas diffusion layer which was then used with liquid electrolyte to demonstrate near-100% utilization.[29] Its dimer and tetramer forms have also been investigated, and had initial capacities of 130 and 240 mAh/g, respectively, but rapid capacity fade. [30,31] Here, LLZO cells with LS cathodes demonstrate up to 67% cathode utilization during their 1st discharge. Rapid capacity fade is observed upon cycling to a lower cutoff voltage of 1.8 V or lower. Increasing the lower cutoff voltage to 2.0 V or higher restricts utilization to only half of the LS carbonyl groups (*ca*. 125 mAh/g; 82% of the single-carbonyl reaction) but enables 160 cycles with over 85 mAh/g capacity retained. These results are encouraging when compared to the previously mentioned liquid quinone cells or hybrid cells with inorganic cathodes with capacities of 110 mAh/g after 50 cycles using $Li_2FeMn_3O_8$,[19] 85 mAh/g after 400 cycles using $LiCoO_2$,[20] and 140 mAh/g after 500 cycles.[22] If side reactions at low voltage can be eliminated and cathode structures optimized to reduce conductive carbon content LLZO hybrid cells enable quinone cathode active materials with competitive specific capacities.

Experimental

The LLZO membranes used in this work were produced though an aqueous tape casting process developed previously.[32] The LLZO powder (MSE Supplies, 500 nm) had a nominal composition of $Li_{6.25}AL_{.25}La_3Zr_2O_{12}$. Lithium carbonate (Sigma Aldrich, 2 wt%) was added to mitigate Li loss during sintering, and MgO (US Research Nanomaterials, 50 nm, 4 wt%) was added to control grain growth. Laminated LLZO sheets were sintered at 1050°C for 2.5 h under flowing argon. The sintered sheets were approximately 120 µm thick, with density > 95% and ionic conductivity $>2x10^{-4}$ S/cm.

Li Mg alloy foil anode (MSE supplies) was attached to the LLZO disk by melting in an Ar-atmosphere glove box. The 10 wt% Mg Li alloy was chosen because it has been shown to enhance wetting on LLZO and improve the critical current density of Li dendrite formation when compared to pure Li.[33] First, a circular Au pad approximately 8.77 mm in diameter was deposited via sputtering on to the anode side of the LLZO membrane to facilitate Li wetting and control the diameter of the anode. Then a small disk of Li alloy foil was gently pressed between the Au-coated side of LLZO and a stainless steel spacer. The stack was placed on a hot plate at 200°C. Melting occurred within 30 seconds and wetting was visible though the translucent LLZO membrane.

LS composite cathodes were made with both poly(ethylene oxide) (PEO) and polyvinylidene fluoride (PVDF) as binders with acetonitrile (ACN) and 2-butanone (MEK) used as solvents, respectively. To make the cathode slurry, LS (Sigma), Super P carbon, binder, and solvent in a mass ratio of 5:4:1:312 were added to a polypropylene bottle along with ZrO_2 milling media and mixed overnight on a roller mill. After mixing, approximately 7 mg of the slurry was dropped and spread onto a 9 mm diameter Al foil disk in an Ar-atmosphere glove box. The composite cathode was then weighed after drying to verify cathode loading. Performance of cells with different binders did not appear to be significantly different. During preliminary

experimentation with LS cathode slurries, it was found that the type of solvent impacts the final cathode composite microstructure. Solvents such as MEK and ACN with low boiling points and fast drying times (<1 minute at 25°C) led to small LS crystallites approximately 10 µm in diameter, while slow drying solvents like NMP (>5 minutes at 60°C) led to growth of large, faceted crystallites that could be over 100 µm long (Figure S1). While in-depth characterization was not performed, the large crystallites performed poorly because of both ionic and electronic transport limitations. The 1,4-naphthoquinone (NQ) cathodes were made using the PVDF and MEK cathode slurry with the same mass ratio as for LS.

Electrolyte (20 µl) was added directly to the dried cathode composite by pipette and allowed to wet the cathode before further assembly. There were 4 organic liquid (OL) and ionic liquid (IL) electrolytes used in this study: 1M $LiPF_6$ in 1:1:1 vol. EC:DMC:DEC ($LiPF_6$ OL, MSE Supplies); 1M LiFSI in 1:1 vol. EC:DMC (LiFSI OL, Solvionic); 1:9 mol. LiFSI:PYR13FSI (LiFSI IL, Solvionic); and 1:9 mol. LiTFSI:PYR13FSI (LiTFSI IL, Solvionic). Batteries were assembled into stainless steel CR2032 coin cells (MTI) with stainless steel spacers and wave springs. Each LLZO cell included a small disk of carbon felt to distribute pressure across the LLZO membrane more evenly.

Liquid cells were assembled with the same stainless steel coin cell cases, Li Mg alloy anode, and LS composite cathode. A commercial polymer membrane (Celgard 2340) was used as a separator. Only the $LiPF_6$ OL electrolyte was used in liquid cells, because LiFSI salt is incompatible with stainless steel and the ILs did not wet the polymer separator well. No carbon felt spacer was required for the liquid cells.

Battery cell impedance was characterized with electrochemical impedance spectroscopy using a Biologic VSP-300 potentiostat with a frequency range of 7 MHz to 100 mHz and a perturbation voltage of 10 mV. The same potentiostat was used to record a 72 h open circuit voltage hold. Battery cycling was performed with an Arbin 21084 battery testing system in a TestEquity TEC1 thermal chamber set to 25°C. The cycling schedule for all cells, regardless of voltage window, was 25 cycles at 20 µA followed by 10 cycles each at 25, 30, 40, and then 10 µA. For the LS cells, these currents corresponded to C-rates of 0.24, 0.30, 0.36, 0.48, and 0.12 respectively. 20 µA is equivalent to 33 $\mu A/cm^2$.

Results/Discussion

Comparison of LLLZO Hybrid and Liquid Cells

The benefits of using an LLZO sheet as an impermeable membrane to prevent dissolved lawsone transport to the anode were first confirmed by comparing a liquid electrolyte cell with a porous polymer separator to hybrid cells with an LLZO separator and liquid catholyte. The superior cycling performance of the LLZO hybrid cell is immediately apparent (Figure 1a). The LLZO cell with LiTFSI IL catholyte had an initial discharge capacity of 312 mAh/g (101% of the 307 mAh/g theoretical 2 e^- reversible reaction capacity, Figure 1c) which fell to 231 mAh/g (83%) by the 10^{th} cycle and 115 mAh/g (41%) by the 50^{th}. In contrast, the cell with the $LiPF_6$ OL electrolyte and a Celgard separator reached just 85 mAh/g (30.3%) in its first

discharge and rapidly faded to only 8% by the 10th discharge cycle. Photographs of a disassembled cell (Figure 1e) clearly show the spread of dissolved lawsone into the separator and crossover to the anode surface, where it is known to react with Li.[30] Presumably, the low initial capacity is due to crossover occurring between cell assembly and operation. These cells both used the PEO-based cathode slurry and were cycled with 3.2 V and 1.8 V upper and lower cutoff voltages, respectively, at rates from 0.12 C to 0.48 C based on the full theoretical capacity of lawsone undergoing the reversible 2 e^- reaction (Figure 1c).

Open-circuit voltage holds for liquid and LLZO cells as-assembled further demonstrate the ability of LLZO to prevent self-discharge by blocking transport of the soluble lawsone (Figure 1b). In the liquid cell, the OCV drops rapidly from 2.8V associated with lithiation of the hydroxyl group[29], to approximately 2.4 V for lithiation of the 1st carbonyl group after approximately 4 h. In contrast, the OCV of the LLZO cell with LiTFSI IL is relatively stable for 72 h. These comparisons to liquid cells illustrated the advantages of using the solid LLZO separator, and liquid cells were not pursued further.

During cycling, the initial discharge capacity of the LLZO cell exceeds 100%. This is expected because of irreversible lithiation of lawsone's hydroxyl group around 2.8 V. However, theoretical capacity in the case of the full 3 e^- reaction is 462 mAh/g. That means the utilization of cathode material is only about 67% on the first discharge. This is supported by examining the voltage behavior on in the 1st discharge (Figure 1 d) as the plateaus attributed to the carbonyl groups' lithiation (2.35 and 2.0 V) account for about 2/3 of the total discharge capacity as would be expected. Another notable feature is that the hydroxyl group lithiation at 2.8 V, which was thought to be irreversible, appears in both charge and discharge curves through 40 cycles before disappearing by cycle 50. The persistence of the hydroxyl group lithiation and de-lithiation is a feature of IL catholytes with both LiTFSI and LiFSI salts and is discussed in the next section which compares the performance of several catholytes.

Interestingly, the coulombic efficiency of both cells was above 100% for the duration tested (Figure S2). This phenomenon is seen in all the lawsone cells tested. Efficiency over 100% may be expected during the initial cycles because of the effects of irreversible hydroxyl group lithiation, but the high efficiency persists after the hydroxyl group plateau has stopped appearing in discharge curves. Evidence from varying the lower cutoff voltages, presented in a later section, suggests this is partially caused by a reduction side reaction at low voltages. The potential liberation of H^+ during hydroxyl group lithiation may also contribute. This is supported by comparison to the near-100% efficiency of cells with NQ, which do not contain a hydroxyl group, discussed below. Assembly of cells in the charged state and cathode material utilization below 100% may also contribute. As cycling proceeds, unused cathode material may become accessible *via* dissolution or other means, which can then be lithiated on discharge. Detailed identification of the mechanisms is left for future work.

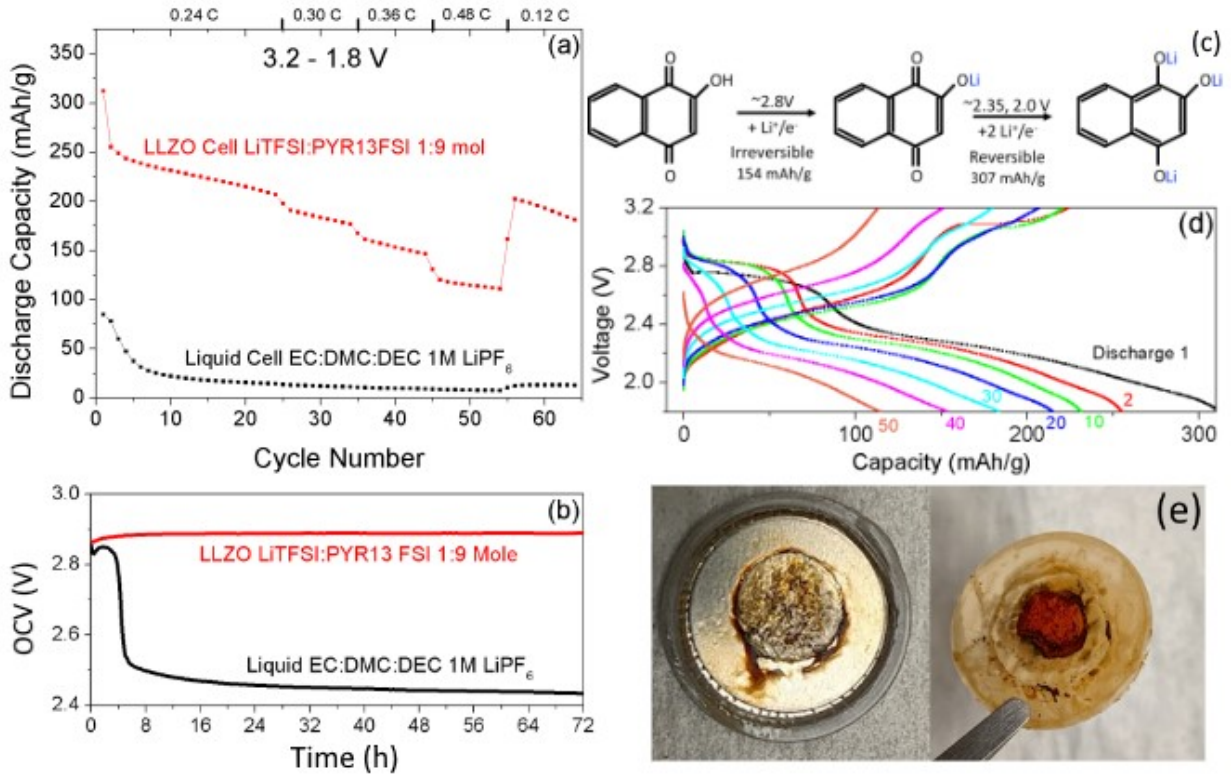

Figure 1: Comparison of liquid-soaked Celgard and solid LLZO separators. *Performance of Li|Lawsone battery cells in both hybrid LLZO solid-separator/liquid-catholyte and full liquid-electrolyte configurations. (a) Cycling performance of a liquid cell and an LLZO cell at several rates. (b) Self-discharge OCV holds over 72 hours. (c) An illustration of the lawsone lithiation reactions.[29] (d) charge/discharge curves at several rates of an LLZO cell with 1:9 mol. LiTFSI: PYR13FSI electrolyte. Cycles 1, 2, 10 and 20 have a rate of 0.24 C while cycles 30, 40, and 50 are at 0.30 C, 0.46 C, and 0.12 C respectively. (e) Photographs of the damaged Li anode (left) and Celgard separator (right) from a cycled liquid cell.*

Catholyte Analysis

Two organic liquid and two ionic liquid catholytes were tested in LLZO cells to determine the sensitivity of cell performance to both the catholyte Li salt and solvent. The IL and OL catholytes each had a characteristic cycling behavior, independent of the type of Li salt (Figure 2a). Cells with an OL catholyte are characterized by rapid capacity fade within the first 15 cycles, followed by more gradual fade thereafter. The IL cells had better initial stability with fade accelerating thereafter, particularly after the 55th cycle. The LiTFSI IL described in the previous section provided the best performance. The best performing OL catholyte was $LiPF_6$ EC:DMC:DEC, which had an initial discharge capacity of 355 mAh/g (127% of the 2 e^- reaction) which fell to 182 mAh/g (65%) by the 10th cycle and 125 mAh/g (45%) by the 50th. Some of the differences in the early cycling behavior between the IL and OL catholytes are related to the lithiation and delithiation behavior of the hydroxyl group. The cells with IL catholytes appear to have higher capacity because they can charge the hydroxyl group through more cycles than OL cells. This can be seen in the differential capacity curves above approximately 2.8 V (Figure 2b, c). In the IL cell at *ca.* 2.35 V, the 1st carbonyl discharge peak has a broad shoulder at lower voltage, unlike the OL cell which initially has a shoulder on the high voltage side

that eventually splits to a separate peak as cycling proceeds. Another difference is the behavior of the 2nd carbonyl reduction peak at approximately 1.9 to 2.0 V. In the IL cell there is an activation of that peak during the first 10-20 cycles, before it starts to fade. In the OL cell this peak fades away during discharge by the 10th cycle. Low utilization of the 2nd carbonyl lithiation below 2 V, as indicated by the low peak area, appears to be a key driver of the low total capacity.

OL cells appear to have better capacity retention at higher rates than the IL cells (Figure 2a and Figure S3) because of lower overall cell impedance, even though they have very high initial fade. For example, the $LiPF_6$ OL cell has a seven-fold lower impedance than the LiTFSI IL cell (Figure 3). When the rate is increased from 0.24 C to 0.30 C the difference in impedance is, in part, responsible for the LiTFSI IL cell losing 6.1% capacity while the OL $LiPF_6$ cell only loses 1.3%. Both cells' total impedance changes minimally over cycling, but growth of the high frequency semicircles indicates a degradation of the ionic conductivity of the LLZO and the LLZO|catholyte interface (insets Figure 3 and Figure S4). The first high-frequency semicircle, attributed to LLZO bulk ionic conductivity, increased by 73% and 14% upon cycling for $LiPF_6$ OL and LiTFSI IL, respectively. These findings are consistent with previous observations that LLZO/electrolyte interactions are sensitive to the electrolyte salt composition, and that $LiPF_6$ reacts more severely than LiTFSI.[34–36] The present data suggests LiFSI is nearly as reactive as $LiPF_6$ and interface degradation is tentatively proposed as the reason the LiFSI IL faded more rapidly than the LiTFSI IL, but further study is warranted.

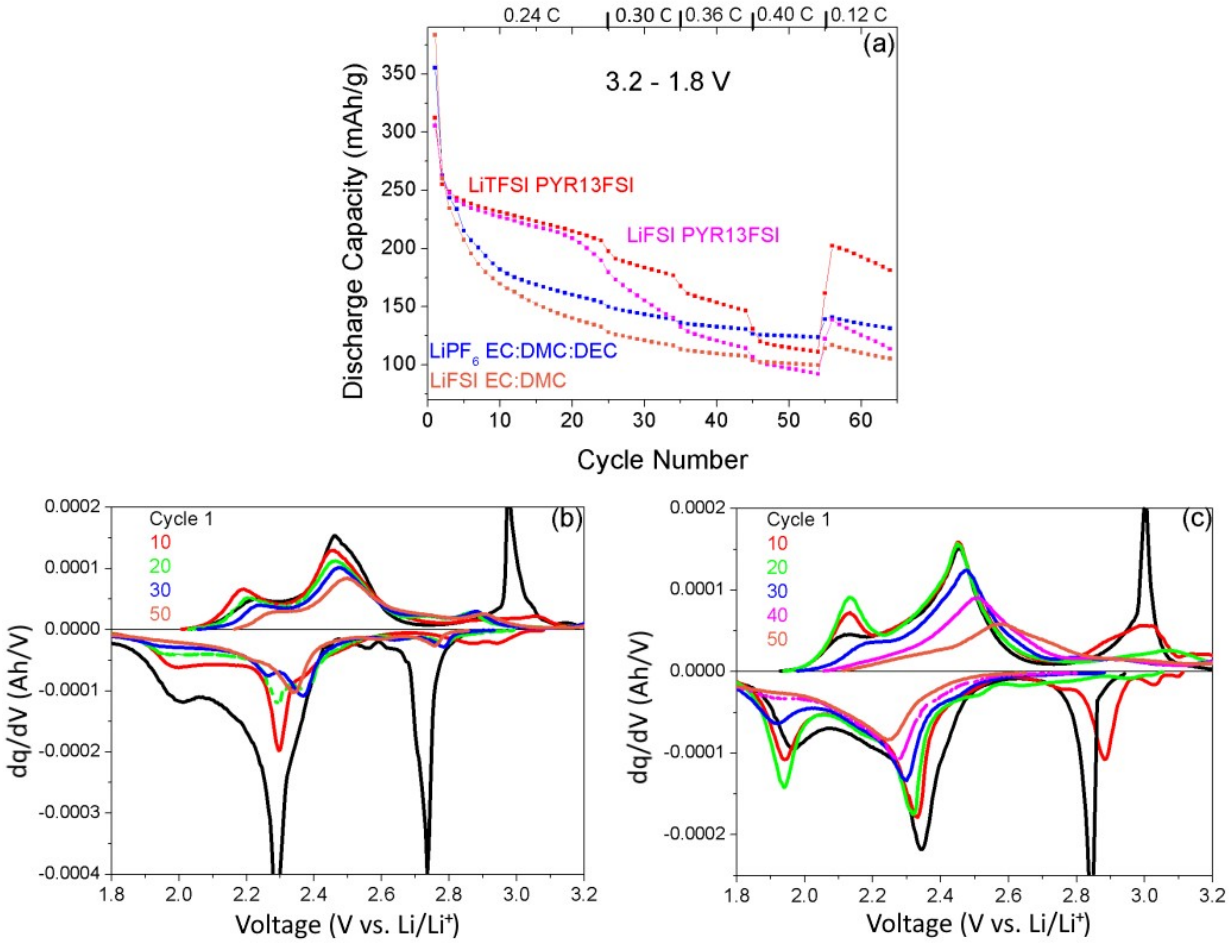

Figure 2: Impact of catholyte. *(a) Performance of LLZO cells with several different liquid catholytes. Charge/discharge differential capacity curves for a cell with (b) EC:DMC and 1M LiFSI, and (c) LiFSI:PYR13FSI.*

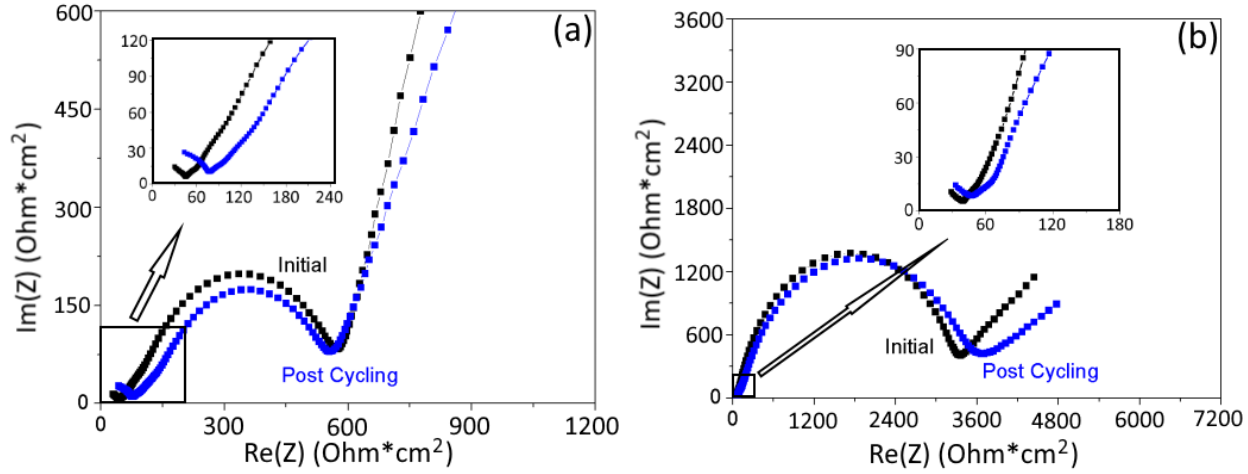

Figure 3: Catholyte Impedance*: Nyquist plotsof LLZO cells before and after cycling with (a) LiPF6 EC:DMC:DEC and (b) LiTFSI PYR13FSI.*

Voltage Window Examination

To probe LLZO cell degradation mechanisms, cells with LiTFSI IL catholyte and PVDF-based cathode slurry were cycled to several different lower cutoff voltages (LCV, Figure 4). These cells were also operated with an upper cutoff voltage of 2.8 V to eliminate effects of charging and discharging the hydroxyl group after the 1st discharge (complete charge and discharge curves are shown in Figure S5). They were run at the same rates as the previous cells, with an additional 100 cycles at 0.24 C added for the 2.0 and 2.1 V LCV cells after the original cycling schedule was complete. Cutoff voltages of 1.6 V and 1.8 V cause accelerated degradation, leading to a dramatic drop in capacity starting after about 20 and 40 cycles, respectively. For cutoff voltages of 2.0 V or greater, the fade is significantly slower. The 1.6 V LCV cell faded from 175 mAh/g in its 2nd cycle to 58 mAh/g by the 65th cycle (33% retained), whereas the 2.1 V cell started at 118 mAh/g and retained 113 mAh/g capacity (96%) after 65 cycles and 88 mAh/g (74%) after 165 cycles. Clearly, discharging below 2 V damages the cell, and a possible mechanism is discussed below.

Differential capacity plots of the 20th and 60th cycles illustrate the relative stability of the 2.0 V and 2.1 V LCV cells and poor utilization of the 2nd carbonyl lithiation during discharge below 2 V (Figure 5 and Figure S6). For the 1.6 V and 1.8 V LCV cells, the peak heights are reduced significantly during cycling, with only a small voltage shift. This is consistent with active material loss as the main driver of capacity fade, rather than increased impedance which would appear as a voltage shift. In contrast, the 2.0 V and 2.1 V LCV cells show minimal change after cycling. Additionally, these plots confirm that the 2.0 V and 2.1 V cells do not discharge to low enough voltage to utilize the 2nd carbonyl lithiation, as indicated by the absence of the peak around 1.9 V. The relatively small difference in initial capacity for all LCVs illustrates the poor utilization of the 2nd carbonyl lithiation even for the 1.6 V and 1.8 V LCV. If the 1st and 2nd lithiations provided similar capacity, the 1.6 and 1.8 V LCF cells would have approximately twice the capacity of the 2.0 and 2.1 V cells. However, this is not the case; the 1.6 V cell has only about 40% more capacity than the 2.1 V cell.

Coulombic efficiency generally increased further above 100% with decreased cutoff voltage. This trend is expected if one of the primary drivers of efficiency above 100% is a reduction side reaction on the cathode side of the cell, which would be exacerbated at low voltage. Such side reaction would lead to longer discharge times and provide an internal charging mechanism thereby reducing the amount of external charge required on charge. It should be noted that efficiency was slightly above 100% even in the 2.1 and 2.0 V LCV cells, indicating this issue is not completely avoided at those higher LCVs.

Taken together, these results suggest that a reduction side reaction at low cell voltage consumes LS active material, and manifests as a rapid capacity fade and coulombic efficiency exceeding 100%. To curtail this reaction, a higher LCV can be used but this comes at the expense of incomplete utilization of the 2nd carbonyl lithiation and therefore lower total capacity. Further work should focus on identifying the side reaction mechanism and products. A solution to this issue is

anticipated to mitigate capacity fade and increase capacity by enabling a lower LCV which would improve utilization of the 2nd lithiation.

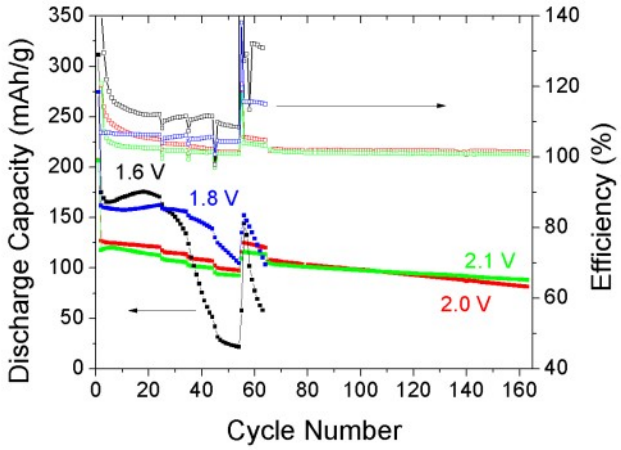

Figure 4: Impact of lower cutoff voltage. *Cycling performance of LS LLZO cells with LiTFSI:PYR13FSI catholyte using an upper cutoff voltage of 2.8 V and lower cutoff voltages varied between 1.6 and 2.1 V.*

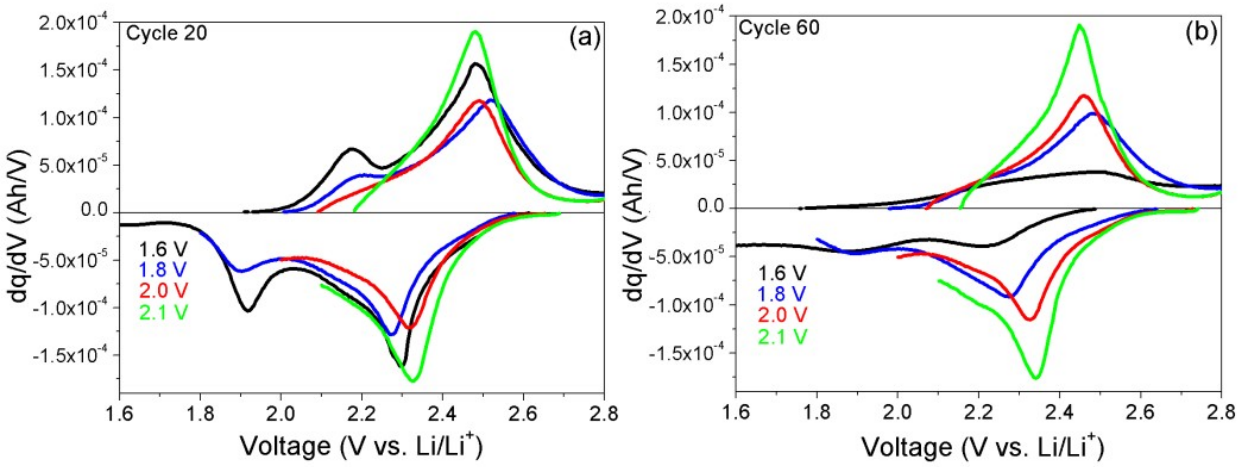

Figure 5: Analysis of lower cutoff voltage. *Differential capacity of LS LLZO cells with LiTFSI:PYR13FSI catholyte with lower cutoff voltages between 1.6 and 2.1 V in the (a) 20th cycle and (b) 60th cycle.*

1,4-Naphthoquinone

NQ is structurally identical to LS except for the absence of the hydroxyl group and is used here to verify assignment of the 2.8 V plateau to lithiation of the hydroxyl group in the LS cells. Furthermore, eliminating the hydroxyl group removes both a source of irreversible lithiation and a potential cause of reductive side reactions stemming from the liberation of a hydrogen atom. Figure 6a shows cycling performance of an LLZO cell with an NQ cathode and LiFSI OL catholyte. The first discharge of the cell at 0.13 C had a capacity of 84 mAh/g which is 24.7% of the 339 mAh/g theoretical capacity, and notably worse utilization than LS LLZO cells. Discharge capacity faded to 66 mAh/g in the 2nd cycle and 58 mAh/g in the 10th.

Capacity fade in later cycles does not accelerate, in contrast to LS cells with LCVs of 1.8 V or lower. The NQ cell lost only 0.7 mAh/g over 10 cycles at 0.26 C, and capacity increased slightly over the last 10 cycles at 0.07 C. It appears that NQ cells are not subject to the same degradation mechanisms as LS cells, although their cathode material utilization is sizably worse. NQ has much lower ionic and electronic conductivity than LS, and that may contribute to the large difference in utilization.[29] Coulombic efficiency is 95% in the 2nd cycle and rises to 100.6% in the 4th before slowly falling back to 100.0 by the 50th cycle.

The voltage profiles confirm assignment of the 2.8 V plateau in LS cells to hydroxyl group lithiation (Figure 6b). When the NQ and LS profiles are compared, there is an additional plateau for the LS cells (at approximately 2.8V discharge and 3 V charge) that fades quickly to become irreversible, as expected. In contrast, the highest-voltage plateau for the NQ cell occurs at lower voltage and cycles continuously. The voltage profiles for NQ are, however, more complicated than expected for the anticipated 2 e- reaction. Three plateaus are visible between 2.7 V and 2.4 V, along with another below 2.0 V. This matches neither the expected voltages of 2.38 V and 2.29 V found from density functional theory calculations[3] or 2.52 V and 2.32 V found experimentally in liquid cells.[29] Further analysis was not pursued as NQ is not an attractive cathode material due to its poor ionic and electronic conductivity.

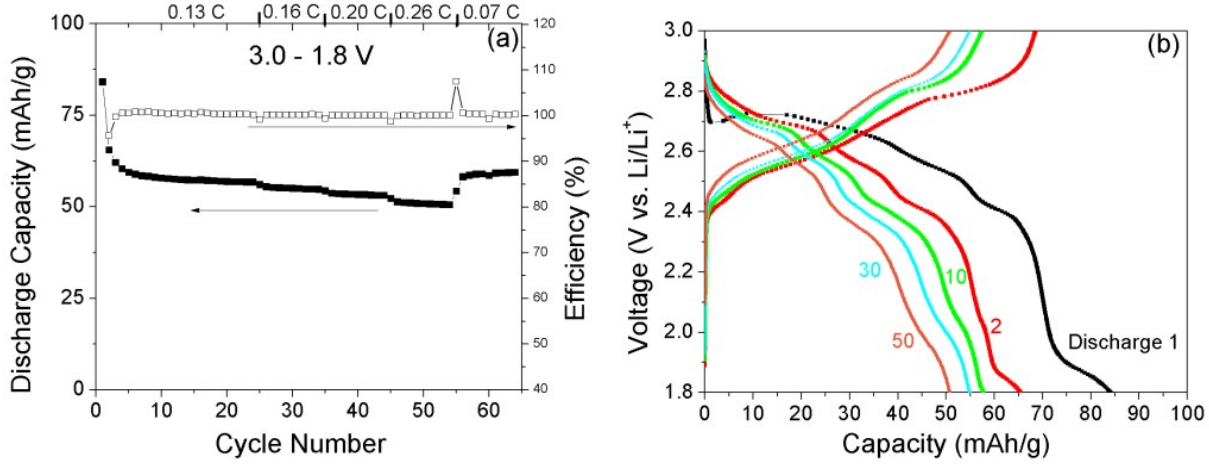

Figure 6: 1,4-Napthoquinone performance. *(a) Cycling performance and (b) charge/discharge curves of NQ cells with 1M LiFSI in EC:DEC catholyte.*

Conclusions

This work serves as a proof-of-concept for using LLZO as an impermeable separator to enable use of small-molecule organic cathode active materials that are soluble liquid electrolyte and therefore not suitable for conventional Li-ion cell designs. A hybrid cell with solid LLZO separator and liquid catholyte using the naturally derived quinone lawsone as a cathode active material and LiTFSI IL catholyte achieved approximately 67% cathode utilization in its first discharge and demonstrated low self-discharge in a 72 h OCV hold. This cell also cycled 25 times at 0.24 C with a capacity over 200 mAh/g, which is 66% of the theoretical reversible 2 e^-/2 Li reaction capacity for LS. LS LLZO cells are also noted to have coulombic efficiencies

above 100% throughout most of their cycling schedules which is thought to be driven by a combination of irreversible hydroxyl group lithiation, unreacted cathode material, and side reactions. Examination of lower cutoff voltages between 1.6 and 2.1 V for cycling cells identified that a side reaction taking place below 2.0 V is responsible for rapid capacity fade. Lower LCVs were also found to correlate with higher coulombic efficiencies over 100%. Although an LCV of 2.0 V or higher enables long-term stability over 165 cycles, it prevents access to the capacity of the 2nd carbonyl group on LS. Common among all the LS cells is the lithiation of the hydroxyl group on LS, either in the first cycle or over several initial cycles. This reaction potentially liberates a proton which may play a role in the observed coulombic efficiency and capacity fade. The behavior of a similar cell with NQ cathode, which lacks the hydroxyl group, supports this hypothesis as the capacity fade is lower and efficiency is closer to 100%. Otherwise, NQ is a poor cathode candidate. Given these findings, future work with LLZO separator and small-molecule quinone cathodes should focus on determining a cost-effective catholyte compatible with LLZO, identifying quinones with good electronic and ionic transport properties or developing cathode composite architectures that mitigate transport issues, and on avoiding molecules with functional groups subject to irreversible lithiation.

ASSOCIATED CONTENT

Supporting Information (PDF file):

SEM images of as-deposited cathodes; comparison of coulombic efficiency of a liquid cell and several LLZO hybrid cells; charge/discharge curves of LLZO cells with several catholyte compositions; impedance spectra of LLZO cells with LiFSI IL and LiFSI OL catholytes; charge/discharge curves or LLZO cells with LiTFSI IL catholyte cycled at lower cutoff voltage from 1.6 V-2.1 V; differential capacity plots of LLZO cells with lower cutoff voltages from 1.6 V–2.1 V

Author Information

Corresponding Author

Michael C. Tucker − Lawrence Berkeley National Laboratory, Berkeley, California; orcid.org/0000-0002-8508-499X; E-mail: mctucker@lbl.gov

Other Authors

Robert A. Jonson − Lawrence Berkeley National Laboratory, Berkeley, California; orcid.org/0000-0001-9314-4609

Vincent S. Battaglia - Lawrence Berkeley National Laboratory, Berkeley, California; https://orcid.org/0000-0002-5596-9148

Notes

The authors declare no competing financial interest.

Acknowledgements

This work was supported by the Vehicle Technologies Office, Office of Energy Efficiency and Renewable Energy, of the U.S. Department of Energy. The authors thank Fengyu Shen, Simon Thompson, and Peter Faguy for helpful discussion. This work was funded in part by the U.S. Department of Energy under contract no. DE-AC02-05CH11231. The views and opinions of the authors expressed herein do not necessarily state or reflect those of the United States Government or any agency thereof. Neither the United States Government nor any agency thereof, nor any of their employees, makes any warranty, expressed or implied, or assumes any legal liability or responsibility for the accuracy, completeness, or usefulness of any information, apparatus, product, or process disclosed, or represents that its use would not infringe privately owned rights.

Funding

All authors received funding from U.S. Department of Energy contract number DE-AC02-05CH11231.

References

(1) Son, E. J.; Kim, J. H.; Kim, K.; Park, C. B. Quinone and Its Derivatives for Energy Harvesting and Storage Materials. *Journal of Materials Chemistry A* **2016**, *4* (29), 11179–11202. https://doi.org/10.1039/c6ta03123d.

(2) Wu, Y.; Zeng, R.; Nan, J.; Shu, D.; Qiu, Y.; Chou, S.-L. Quinone Electrode Materials for Rechargeable Lithium/Sodium Ion Batteries. *Advanced Energy Materials* **2017**, *7* (24). https://doi.org/10.1002/aenm.201700278.

(3) Miao, L.; Liu, L.; Shang, Z.; Li, Y.; Lu, Y.; Cheng, F.; Chen, J. The Structure-Electrochemical Property Relationship of Quinone Electrodes for Lithium-Ion Batteries. *Phys Chem Chem Phys* **2018**, *20* (19), 13478–13484. https://doi.org/10.1039/c8cp00597d.

(4) Häupler, B.; Wild, A.; Schubert, U. S. Carbonyls: Powerful Organic Materials for Secondary Batteries. *Advanced Energy Materials* **2015**, *5* (11), 1402034. https://doi.org/10.1002/aenm.201402034.

(5) Nokami, T.; Matsuo, T.; Inatomi, Y.; Hojo, N.; Tsukagoshi, T.; Yoshizawa, H.; Shimizu, A.; Kuramoto, H.; Komae, K.; Tsuyama, H.; Yoshida, J. Polymer-Bound Pyrene-4,5,9,10-Tetraone for Fast-Charge and -Discharge Lithium-Ion Batteries with High Capacity. *J. Am. Chem. Soc.* **2012**, *134* (48), 19694–19700. https://doi.org/10.1021/ja306663g.

(6) Cao, S.; Zhang, H.; Zhao, Y.; Zhao, Y. Pillararene/Calixarene-Based Systems for Battery and Supercapacitor Applications. *eScience* **2021**, *1* (1), 28–43. https://doi.org/10.1016/j.esci.2021.10.001.

(7) Senoh, H.; Yao, M.; Sakaebe, H.; Yasuda, K.; Siroma, Z. A Two-Compartment Cell for Using Soluble Benzoquinone Derivatives as Active Materials in Lithium Secondary Batteries. *Electrochimica Acta* **2011**, *56* (27), 10145–10150. https://doi.org/10.1016/j.electacta.2011.08.115.

(8) Ramakumar, S.; Deviannapoorani, C.; Dhivya, L.; Shankar, L. S.; Murugan, R. Lithium Garnets: Synthesis, Structure, Li + Conductivity, Li + Dynamics and Applications. *Progress in Materials Science* **2017**, *88*, 325–411. https://doi.org/10.1016/j.pmatsci.2017.04.007.

(9) Wang, C.; Fu, K.; Kammampata, S. P.; McOwen, D. W.; Samson, A. J.; Zhang, L.; Hitz, G. T.; Nolan, A. M.; Wachsman, E. D.; Mo, Y.; Thangadurai, V.; Hu, L. Garnet-Type Solid-State Electrolytes: Materials, Interfaces, and Batteries. *Chem Rev* **2020**, *120* (10), 4257–4300. https://doi.org/10.1021/acs.chemrev.9b00427.
(10) Wolfenstine, J.; Allen, J. L.; Read, J.; Sakamoto, J. Chemical Stability of Cubic Li7La3Zr2O12 with Molten Lithium at Elevated Temperature. *Journal of Materials Science* **2013**, *48* (17), 5846–5851. https://doi.org/10.1007/s10853-013-7380-z.
(11) Wang, J.; Huang, G.; Zhang, X.-B. Interface between Lithium Metal and Garnet Electrolyte: Recent Progress and Perspective. *Batteries & Supercaps* **2020**, *3* (10), 1006–1015. https://doi.org/10.1002/batt.202000082.
(12) Thompson, T.; Yu, S.; Williams, L.; Schmidt, R. D.; Garcia-Mendez, R.; Wolfenstine, J.; Allen, J. L.; Kioupakis, E.; Siegel, D. J.; Sakamoto, J. Electrochemical Window of the Li-Ion Solid Electrolyte Li7La3Zr2O12. *ACS Energy Letters* **2017**, *2* (2), 462–468. https://doi.org/10.1021/acsenergylett.6b00593.
(13) Miara, L. J.; Richards, W. D.; Wang, Y. E.; Ceder, G. First-Principles Studies on Cation Dopants and Electrolyte|Cathode Interphases for Lithium Garnets. *Chemistry of Materials* **2015**, *27* (11), 4040–4047. https://doi.org/10.1021/acs.chemmater.5b01023.
(14) Rangasamy, E.; Wolfenstine, J.; Sakamoto, J. The Role of Al and Li Concentration on the Formation of Cubic Garnet Solid Electrolyte of Nominal Composition Li7La3Zr2O12. *Solid State Ionics* **2012**, *206*, 28–32. https://doi.org/10.1016/j.ssi.2011.10.022.
(15) Zhao, Y.; Guo, J. Development of Flexible Li-Ion Batteries for Flexible Electronics. *InfoMat* **2020**, *2* (5), 866–878. https://doi.org/10.1002/inf2.12117.
(16) Nie, K.; Hong, Y.; Qiu, J.; Li, Q.; Yu, X.; Li, H.; Chen, L. Interfaces Between Cathode and Electrolyte in Solid State Lithium Batteries: Challenges and Perspectives. *Front. Chem.* **2018**, *6*, 616. https://doi.org/10.3389/fchem.2018.00616.
(17) Ren, Y.; Liu, T.; Shen, Y.; Lin, Y.; Nan, C.-W. Chemical Compatibility between Garnet-like Solid State Electrolyte Li6.75La3Zr1.75Ta0.25O12 and Major Commercial Lithium Battery Cathode Materials. *Journal of Materiomics* **2016**, *2* (3), 256–264. https://doi.org/10.1016/j.jmat.2016.04.003.
(18) Kim, K. J.; Rupp, J. L. M. All Ceramic Cathode Composite Design and Manufacturing towards Low Interfacial Resistance for Garnet-Based Solid-State Lithium Batteries. *Energy Environ. Sci.* **2020**, *13* (12), 4930–4945. https://doi.org/10.1039/D0EE02062A.
(19) Han, X.; Gong, Y.; Fu, K. (Kelvin); He, X.; Hitz, G. T.; Dai, J.; Pearse, A.; Liu, B.; Wang, H.; Rubloff, G.; Mo, Y.; Thangadurai, V.; Wachsman, E. D.; Hu, L. Negating Interfacial Impedance in Garnet-Based Solid-State Li Metal Batteries. *Nature Mater* **2017**, *16* (5), 572–579. https://doi.org/10.1038/nmat4821.
(20) Bi, Z.; Zhao, N.; Ma, L.; Fu, Z.; Xu, F.; Wang, C.; Guo, X. Interface Engineering on Cathode Side for Solid Garnet Batteries. *Chemical Engineering Journal* **2020**, *387*, 124089. https://doi.org/10.1016/j.cej.2020.124089.
(21) Yi, E.; Shen, H.; Heywood, S.; Alvarado, J.; Parkinson, D. Y.; Chen, G.; Sofie, S. W.; Doeff, M. M. All-Solid-State Batteries Using Rationally Designed Garnet Electrolyte Frameworks. *ACS Applied Energy Materials* **2020**, *3* (1), 170–175. https://doi.org/10.1021/acsaem.9b02101.
(22) Shao, Y.; Wang, H.; Gong, Z.; Wang, D.; Zheng, B.; Zhu, J.; Lu, Y.; Hu, Y.-S.; Guo, X.; Li, H.; Huang, X.; Yang, Y.; Nan, C.-W.; Chen, L. Drawing a Soft Interface:

An Effective Interfacial Modification Strategy for Garnet-Type Solid-State Li Batteries. *ACS Energy Lett.* **2018**, *3* (6), 1212–1218. https://doi.org/10.1021/acsenergylett.8b00453.
(23) Li, Y.; Xu, B.; Xu, H.; Duan, H.; Lü, X.; Xin, S.; Zhou, W.; Xue, L.; Fu, G.; Manthiram, A.; Goodenough, J. B. Hybrid Polymer/Garnet Electrolyte with a Small Interfacial Resistance for Lithium-Ion Batteries. *Angewandte Chemie International Edition* **2017**, *56* (3), 753–756. https://doi.org/10.1002/anie.201608924.
(24) Mikhaylik, Y. V.; Akridge, J. R. Polysulfide Shuttle Study in the Li/S Battery System. *Journal of The Electrochemical Society* **2004**, *151* (11). https://doi.org/10.1149/1.1806394.
(25) Hitz, G. T.; McOwen, D. W.; Zhang, L.; Ma, Z.; Fu, Z.; Wen, Y.; Gong, Y.; Dai, J.; Hamann, T. R.; Hu, L.; Wachsman, E. D. High-Rate Lithium Cycling in a Scalable Trilayer Li-Garnet-Electrolyte Architecture. *Materials Today* **2019**, *22*, 50–57. https://doi.org/10.1016/j.mattod.2018.04.004.
(26) Fu, K.; Gong, Y.; Hitz, G. T.; McOwen, D. W.; Li, Y.; Xu, S.; Wen, Y.; Zhang, L.; Wang, C.; Pastel, G.; Dai, J.; Liu, B.; Xie, H.; Yao, Y.; Wachsman, E. D.; Hu, L. Three-Dimensional Bilayer Garnet Solid Electrolyte Based High Energy Density Lithium Metal–Sulfur Batteries. *Energy & Environmental Science* **2017**, *10* (7), 1568–1575. https://doi.org/10.1039/c7ee01004d.
(27) Huang, X.; Liu, C.; Lu, Y.; Xiu, T.; Jin, J.; Badding, M. E.; Wen, Z. A Li-Garnet Composite Ceramic Electrolyte and Its Solid-State Li-S Battery. *Journal of Power Sources* **2018**, *382*, 190–197. https://doi.org/10.1016/j.jpowsour.2017.11.074.
(28) Naguib, M.; Sharafi, A.; Self, E. C.; Meyer, H. M.; Sakamoto, J.; Nanda, J. Interfacial Reactions and Performance of Li7La3Zr2O12-Stabilized Li-Sulfur Hybrid Cell. *ACS Appl Mater Interfaces* **2019**, *11* (45), 42042–42048. https://doi.org/10.1021/acsami.9b11439.
(29) Lee, J.; Park, M. J. Tattooing Dye as a Green Electrode Material for Lithium Batteries. *Advanced Energy Materials* **2017**, *7* (12). https://doi.org/10.1002/aenm.201602279.
(30) Miroshnikov, M.; Kato, K.; Babu, G.; Divya, K. P.; Reddy Arava, L. M.; Ajayan, P. M.; John, G. A Common Tattoo Chemical for Energy Storage: Henna Plant-Derived Naphthoquinone Dimer as a Green and Sustainable Cathode Material for Li-Ion Batteries. *RSC Adv* **2018**, *8* (3), 1576–1582. https://doi.org/10.1039/c7ra12357d.
(31) Miroshnikov, M.; Kato, K.; Babu, G.; Thangavel, N. K.; Mahankali, K.; Hohenstein, E.; Wang, H.; Satapathy, S.; Divya, K. P.; Asare, H.; Ajayan, P. M.; Arava, L. M. R.; John, G. Made From Henna! A Fast-Charging, High-Capacity, and Recyclable Tetrakislawsone Cathode Material for Lithium Ion Batteries. *ACS Sustainable Chemistry & Engineering* **2019**, *7* (16), 13836–13844. https://doi.org/10.1021/acssuschemeng.9b01800.
(32) Jonson, R. A.; Yi, E.; Shen, F.; Tucker, M. C. Optimization of Tape Casting for Fabrication of Li6.25Al0.25La3Zr2O12 Sheets. *Energy & Fuels* **2021**, *35* (10), 8982–8990. https://doi.org/10.1021/acs.energyfuels.1c00566.
(33) Yang, C.; Xie, H.; Ping, W.; Fu, K.; Liu, B.; Rao, J.; Dai, J.; Wang, C.; Pastel, G.; Hu, L. An Electron/Ion Dual-Conductive Alloy Framework for High-Rate and High-Capacity Solid-State Lithium-Metal Batteries. *Adv Mater* **2019**, *31* (3), e1804815. https://doi.org/10.1002/adma.201804815.
(34) Gupta, A.; Kazyak, E.; Dasgupta, N. P.; Sakamoto, J. Electrochemical and Surface Chemistry Analysis of Lithium Lanthanum Zirconium Tantalum Oxide

(LLZTO)/Liquid Electrolyte (LE) Interfaces. *Journal of Power Sources* **2020**, *474*. https://doi.org/10.1016/j.jpowsour.2020.228598.
(35) Schleutker, M.; Bahner, J.; Tsai, C. L.; Stolten, D.; Korte, C. On the Interfacial Charge Transfer between Solid and Liquid Li(+) Electrolytes. *Phys Chem Chem Phys* **2017**, *19* (39), 26596–26605. https://doi.org/10.1039/c7cp05213h.
(36) Liu, J.; Gao, X.; Hartley, G. O.; Rees, G. J.; Gong, C.; Richter, F. H.; Janek, J.; Xia, Y.; Robertson, A. W.; Johnson, L. R.; Bruce, P. G. The Interface between Li6.5La3Zr1.5Ta0.5O12 and Liquid Electrolyte. *Joule* **2020**, *4* (1), 101–108. https://doi.org/10.1016/j.joule.2019.10.001.

FOR TABLE OF CONTENTS ONLY